Plant specific armadillo repeat kinesin directs organelle transport and microtubule convergence to promote tip growth

Asaka Kanda[1], Kento Otani[1], Taku Takahashi[1], Hiroyasu Motose[1]

[1]Department of Biological Science, Graduate School of Natural Science and Technology, Okayama University, Tsushimanaka 3-1-1, Okayama 700-8530, Japan

Abstract

Tip growth is a highly polarized growth process essential for plant growth and reproduction. However, its molecular mechanism and evolutional significance still remain elusive. Here, we show that plant-specific armadillo-repeat containing kinesin, MpARK1, drives long-range organelle transport and microtubule convergence in tip growing rhizoids in a basal land plant *Marchantia polymorpha*. MpARK1 is required for anterograde transport of the nucleus and plastids to maintain their position during persistent tip growth. Furthermore, MpARK1 participates in microtubule focusing on the apex to stabilize growth direction. MpARK1-dependent rhizoid growth is essential for plant anchorage and soil holding capacity. Thus, ARK might be co-opted to serve as a long-range transporter and intracellular organizer in the primitive rooting structure (rhizoid) for the adaptation to terrestrial environments. Our findings suggest that ARK was comparable to animal anterograde kinesin, challenging the traditional view that actomyosin-based cytoplasmic streaming is a dominant transport mode in plant kingdom.

Introduction

Tip growth is evolutionarily conserved process essential for morphogenesis and reproduction in various organisms. Furthermore, it is an excellent model system to study cell polarity and directional growth[1,2]. During initiation, single growth site is established to form a bulge in the outer surface. The bulge expands to generate a dome-shaped apex followed by a cylindrical shank, causing a filamentous morphology. However, it remains elusive how a growth site is established and maintained. Although the detailed mechanism is uncertain, local activation of ROP (Rho of plant) GTPases participates in growth site determination[3,4] and then actin-myosin-mediated vesicle transport and cytoplasmic streaming are thought to drive tip growth[5,6], whereas microtubule-dependent transport have not been well clarified.

Recent studies demonstrate that kinesins, a family of microtubule-based motor proteins, play key roles in tip growth[7-13]. Several kinesins regulate microtubule organization and dynamics to promote tip growth[7,8]. Especially, kinesin-14 family is diverged in land plants and drives minus end-directed transport of organelles, microtubules, actin filaments, and chromatin, most likely as the counterpart of cytoplasmic dynein in animals[10,11,14,15,16]. Two kinesin-14 subfamilies, KCBP (kinesin-like calmodulin binding protein) and KCH (kinesin with calponin homology domain), drive retrograde transport of the nucleus and plastids in tip-growing protonemal apical cells in a moss *Physcomitrium patens*[10,11]. In animals, plus-end-directed kinesins (kinesin-1, 2, 3) predominantly

drive plus-end-directed, anterograde transport of organelles[17], whereas such kinesin remain unclear in plants.

Plant-specific armadillo-repeat kinesin (ARK) has a N-terminal motor domain followed by the C-terminal tail containing coiled-coil domains and tandem armadillo repeats. Because ARK motor domain is not related to those of other kinesin families, they constitute an ungrouped kinesin family[18,19], implying their unknown evolutional origin and unpredictable function. However, microtubule gliding assay has proved the plus-end directed motor activity of *P. patens* kinesin-ARK-a[9]. Further, RNAi screening has shown that *P. patens* kinesin-ARKs are required for anterograde transport of the nucleus toward the protonema apex[9]. However, ARK function remains unclear because RNAi knockdown did not cause any obvious defect in tip growth.

Molecular genetic studies identified ARK1 of *Arabidopsis thaliana* as a regulator of root hair tip growth[20,21]. *Arabidopsis* has three *ARK* genes, *ARK1-ARK3*, which may redundantly and/or independently function in the cell- and organ-specific manners. The *ark1* mutant has short, branching root hairs and excess endoplasmic microtubules[21]. ARK1 localizes to the growing plus ends of microtubules to promote their catastrophe and growth velocity[7]. ARK1 interacts with NIMA (Never In Mitosis A)-related kinase 6 (NEK6)[21] but they independently function in root hairs[22]. ARK1 interplays with ROP2, ADF1 (a class I ADP ribosylation factor GTPase-activating protein), and atlastin GTPase RHD3 (Root Hair Defective3) to promote root hair growth[23-25]. ARK2 participates in root growth direction[21]. ARK3 localizes to preprophase bands and might be involved in asymmetric cell division in the guard cell lineage[26,27], while its function remains unclear.

Rhizoid is a putative early rooting structure in land plants and is emerging as a new model of tip growth[28,29]. A series of studies in rhizoids of *Marchantia polymorpha*, an early diverging land plant, implies common regulators in both rhizoids and root hairs[30-32]. *M. polymorpha* has several advantages including low genetic redundancy[33] and amenable genetic tools[34,35]. The extensive mutant screening has shown that genes involved in cell wall biogenesis, vesicle transport, and cytoskeleton are required for rhizoid growth in *M. polymorpha*[31]. We found a tubulin kinase MpNEK1 localizes to microtubule foci at the apical dome of rhizoid to direct tip growth through microtubule reorganization[36]. Another microtubule-associated protein, MpWDL (WAVE DAMPENED-LIKE), regulates growth direction of rhizoids by stabilizing microtubules aligned along the longitudinal axis of rhizoids[37]. However, the mechanism of rhizoid growth remains unexplored.

Here, we found that *M. polymorpha* armadillo-repeat kinesin, MpARK1, directs organelle transport and microtubule configuration to promote rhizoid growth. ARK kinesin might be a predominant anterograde transporter and intracellular organizer to promote tip growth of rooting cells in land plants.

Results

Phylogenetic analysis of *ARK* genes

A single ARK gene, Mp*ARK1* (Mp4g06510), was identified in the genome database of the

liverwort *M. polymorpha* (Fig. 1a, b). The cloned cDNA encodes a protein of 883 amino acid residues composed of a kinesin motor domain, a coiled-coil domain, and four tandem armadillo repeats, the well-conserved domain structure of plant specific armadillo-repeat kinesin (Fig. 1b). The cDNA represents the major transcript of Mp*ARK1* (corresponds to Mp4g06510.2, 3, 7), in which the 12th and 13th exons encoding the C-terminal region of coiled-coil domain were spliced out but coiled-coil domain still existed. The relative expression levels of transcripts with or without these exons was shown in Fig. S1a.

Phylogenetic analysis showed that ARKs can be classified into two clades: the AtARK2 and AtARK1 clade (Fig. 1a), consistently with previous studies[19,26]. MpARK1 belongs to the AtARK2 clade like as do ARKs of the moss, *P. patens*, and the basal vascular plant (lycophytes), *Selaginella moellendorffii*, implying that the *ARK2* clade was ancestral. Any algae including charophyte, a sister lineage of land plants, have no *ARK* gene. The early-diverging angiosperm *Amborella trichopoda* has two *ARK* genes, each of which belongs to the AtARK2 or AtARK1 clade, suggesting that the *ARK1* clade diverged at least in angiosperms.

MpARK1 promotes and directs tip growth of rhizoids

To analyze expression pattern of Mp*ARK1*, we generated transgenic lines expressing nuclear-localized Citrine fluorescent protein (Citrine-NLS) under the control of the Mp*ARK1* promoter (Mp*ARK1pro:Citrine-NLS*). The fluorescently labeled nuclei were observed in rhizoids and in the vegetative flat organ, thallus, especially in air pore cells (Fig. 1c), implying the function of Mp*ARK1* in rhizoids and thallus cells.

To address Mp*ARK1* function, we generated mutants of Mp*ARK1* using CRISPR/Cas9 (Fig. 2, Fig. S1b, c). The guide RNAs were designed to target a motor domain (gRNA1) and an armadillo repeat domain (gRNA2). The isolated mutants were designated Mp*ark1-g1* (motor domain) and Mp*ark1-g2* (armadillo repeat), respectively. All mutant lines exhibited same morphological defects in rhizoids (Fig. 2b). In the wild type, rhizoids elongate by tip growth to a filamentous morphology, whereas the Mp*ark1* mutants have very short, curly rhizoids (Fig. 2b). The phenotype was attributed to the severe suppression of tip growth and the defect of growth direction. Collectively, MpARK1 promotes rhizoid elongation and regulates the direction of tip growth.

In the wild type, most rhizoids entered the agar medium to fix thallus on the substratum, whereas Mp*ark1* mutant rhizoids could not reach and penetrate the agar. Thus, Mp*ark1* mutant thallus was easily peeled away from the agar medium, clearly indicating that rhizoids are essential to anchor the plant body in the substratum. On the other, thallus growth and morphology of Mp*ark1* mutants were normal compared with the wild type (Fig. S1b). Thus, Mp*ARK1* is not essential for thallus development.

MpARK1 kinesin motor and armadillo repeats are essential for tip growth

Next, we generated transgenic lines expressing MpARK1-Citrine fusion protein driven by the Mp*ARK1* promoter (Mp*ARK1pro:*Mp*ARK1-Citrine*) in the Mp*ark1-g1* mutant background (Fig. 2c-e). The defect of tip growth was rescued in all transgenic 24 lines expressing MpARK1-Citrine.

Rhizoid growth was equivalent between the wild type and the complementation lines (Fig. 2e).

We next examined function of kinesin motor and armadillo repeats of MpARK1. The C-terminal truncated MpARK1 lacking armadillo repeats (dARM) and a rigor mutant without kinesin motor activity (Rigor) were tagged with Citrine and driven by the Mp*ARK1* promoter in the Mp*ark1-g1* mutant (Fig. 2c, d). The full-length MpARK1 tagged with Citrine recovered the defects of rhizoid growth, whereas both dARM and rigor MpARK1 could not (Fig. 2d). Collectively, both kinesin motor and armadillo repeats are essential for MpARK1 function in rhizoid growth.

MpARK1 localizes to microtubule foci in the apical dome of rhizoids

To assess the subcellular localization of MpARK1, we observed the transgenic lines expressing MpARK1-Citrine by confocal microscopy. MpARK1-Citrine localized to the apical dome of rhizoids, where tip growth takes place (Fig. 3a). MpARK1-Citrine accumulated in particles and along the cytoskeletal filamentous structures. MpARK1 particles moved toward and away from the apex with fusion and separation events (Movie 1, 2, Fig. S2a). The velocity of the apical-directed MpARK1 particles is 4.5±1.1 μm/min, which is almost half of that of basal-directed particles (Fig. S2b). The particles accumulated in the crossovers of filaments to change their position. In contrast, MpARK1 dARM-Citrine localized in the cytoplasm, demonstrating that armadillo repeats are required for apical localization (Fig. 3b).

To examine microtubule localization of MpARK1, we generated double labelled lines expressing both Citrine-MpTUB2 (microtubule marker, *CaMV35Spro:Citrine*-Mp*TUB2*, ref. 36) and MpARK1-TagRFP (Mp*ARK1pro:*Mp*ARK1-TagRFP*). MpARK1-TagRFP localized to microtubule foci at the apex of rhizoids (Fig. 3c, S2c). MpARK1 localized to the microtubule ends and also laterally associated with the sides of microtubules.

Since a previous study has shown that *Arabidopsis* ARK1 localized in the microtubule plus ends[7], we examined co-localization of MpARK1-TagRFP and the plus-end marker END BINDING PROTEIN1 (*CaMV35Spro:*Mp*EB1a-Citrine*). MpARK1-TagRFP did not co-localize with MpEB1a-Citrine (Fig. 3d, S2d). Thus, MpARK1 is not a canonical +TIP protein preferentially accumulating in the plus ends.

We further analyzed the effects of microtubule-depolymerizing drug, oryzalin, and actin filament-depolymerizing drug, latrunculin B (Fig. S2e). Treatment with oryzalin disrupted apical localization of MpARK1-Citrine, resulting in dispersed fluorescence signal in the shank region. By contrast, treatment with latrunculin B did not severely affect the localization of MpARK1-Citrine, still accumulating in the apical dome. Collectively, our results showed that MpARK1 associates with microtubule foci in the rhizoid apex through armadillo repeats.

MpARK1 is required for microtubule convergence in the rhizoid apex

Because *Arabidopsis* ARK1 regulates microtubules in root hairs[7,21], we assumed that MpARK1 also regulates microtubule organization and dynamics. To visualize microtubules in rhizoids, we introduced a microtubule marker Citrine-MpTUB2 or a growing plus-end marker MpEB1a-Citrine in the wild type and Mp*ark1-g1* mutants (Fig. 4).

In the wild type, microtubules were parallel or oblique to the longitudinal axis of rhizoids and converged into the focus at the rhizoid apex (Fig. 4a). On the while, the Mp*ark1* mutants did not form obvious microtubule foci at the apex.

MpEB1a-Citrine moved toward the rhizoid apex to converge on the focus in the wild-type, whereas it did not coalesce at the apex in the Mp*ark1* mutant (Fig 4b, Movie 3, 4). The fluorescent density of MpEB1a-Citrine was decreased in the apical dome of Mp*ark1* rhizoids (Fig. 4c, d). We assessed the direction of MpEB1a-Citrine comets and found its significant dispersion in Mp*ark1* mutants (Fig. 4e). In Mp*ark1*, basal-directed plus ends were increased but apical-directed plus ends were still dominant (Fig. 4f). The velocity of MpEB1a-Citrine comets and catastrophe of plus ends (frequency of growth-to-shrink transition evens) was not altered in Mp*ark1* (Fig. 4g, h). These results indicate that MpARK1 directs microtubule plus ends and regulates microtubule convergence at the rhizoid apex.

We next examined whether MpARK1 regulates apical localization of MpNEK1, a tubulin kinase regulating rhizoid growth direction through the apical microtubule reorganization[36] (Fig. S3). MpNEK1-Citrine localized to microtubule foci in the wild type but dispersed to the shank region in Mp*ark1-g1*, suggesting that MpARK1 regulates microtubule convergence through the transport and localization of MpNEK1.

MpARK1 is required for anterograde organelle transport

We found abnormal localization of plastids and the nucleus in Mp*ark1* rhizoids (Fig. 4a, 4b, 5a). A previous study demonstrates that *P. patens* ARK kinesins are required for the movement of the nucleus to the apical direction of protomema after mitosis[9]. Thus, we analyzed the movement of the nucleus and plastids during rhizoid growth. In the wild type, the nucleus moved toward the rhizoid apex at the same velocity of rhizoid growth and kept the distance about 60-100 μm apart from the apex (Fig. 5a-c, Movie 5). In the Mp*ark1* mutants, nuclei were left behind in the basal region of rhizoids due to the significant decrease of anterograde movement (Fig. 5a-c, Movie 6).

We next analyzed the movement of plastids. In the wild type, plastids showed the back-and-forth movement, but proceeded toward the apex to distribute uniformly from the shank to the apical region (Fig. 4a, 4b, 5a, Movie 5). In the Mp*ark1* mutants, the velocity of plastid movement was severely decreased (Fig. 5d) and most plastids were localized in the basal region behind the nucleus (Fig. 4a, 4b, 5a, 5e, Movie 6). We also observed MpARK1-Citrine signal associated with the nucleus and plastids (Fig. S4a, b). Collectively, MpARK1 is required for anterograde transport of the nucleus and plastids.

We further analyzed localization of mitochondria, vesicles, and vacuoles (tonoplast) by staining with DiOC6, BODIPY-conjugated brefeldin A (BODIPY-BFA), and MDY-64, respectively (Fig. S4c). Interestingly, DiOC6-positive mitochondria and BODIPY-BFA-positive vesicles were preferentially accumulated at the apical dome in the wild type rhizoids, whereas they were dispersed in the Mp*ark1* rhizoids. In the absence of MpARK1, vacuole was more extended to the apical side, resulting in the narrower apical cytosol. Thus, MpARK1 may drive anterograde organelle transport to coordinate their subcellular distribution during rhizoid growth.

MpARK1-mediated rhizoid growth is required for holding the soil and promoting vegetative/reproductive development

To address functional significance of MpARK1-mediated rhizoid growth, we monitored plant growth on the soil. On the agar medium, the vegetative flat organ, thallus, mainly constituting the liverwort body, normally grew in the Mp*ark1* mutant compared with the wild type (Fig. S1a). This is likely due to direct absorption of nutrients and water from thalli and enough humidity in the closed culture plates. These artificial environments may mask the requirement of rhizoids and MpARK1 function.

We planted the wild type, Mp*ark1-g1* and Mp*ark1-g2* mutants, and Mp*ark1-g1* mutants introduced with full length, dARM, and rigor MpARK1 tagged with Citrine on the soil (Fig. 6a). Thallus growth was suppressed in Mp*ark1-g1* and Mp*ark1-g2*, whereas recovered in the Mp*ark1-g1* expressing full length MpARK1-Ctrine. The growth suppression could not be rescued in Mp*ark1-g1* introduced with dARM or rigor MpARK1.

We next monitored soil-holding capacity by lifting thalli up in the air (Fig. 6b). Comparing with the wild type and Mp*ark1-g1* complemented with full length MpARK1, Mp*ark1-g1*, Mp*ark1-g2* and Mp*ark1-g1* introduced with dARM or rigor MpARK1 exhibited severely reduced soil-holding capacity, implying that the growth suppression is attributed to the reduced capacity holding the soil and the resulting defect in absorption of nutrients and water.

We next examined reproductive development (Fig. 6c). The wild type and Mp*ark1-g1* complemented with MpARK1 developed fully grown reproductive organ (antheridiophore, male sexual organ), whereas Mp*ark1* mutants and Mp*ark1-g1* introduced with dARM or rigor MpARK1 showed severe dwarf phenotype of antheridiophores. Thus, MpARK1 is required for reproductive development.

To examine the functional conservation of ARK kinesins in tip growth, we introduced MpARK1 in *Arabidopsis ark1 ark2 ark3* triple mutant, which exhibits short, branched root hairs. The defect of root-hair tip growth was rescued by MpARK1 (Fig. S5), suggesting the conserved ARK function in tip growth of rooting cells in land plants.

Discussion

Here, we show that the basal land plant *M. polymorpha* has a single ARK kinesin (MpARK1), which is essential to promote tip growth of rhizoids, the ancestral rooting system in land plants. Our study provides novel insights on the fundamental function of this plant-unique kinesin because most land plants, including mosses, lycophytes, and angiosperms, have multiple *ARK* genes, which redundantly work in plant development and microtubule-dependent processes.

Mp*ark1* mutants showed severe growth defects in rhizoids: suppression of rhizoid elongation and fluctuation of growth direction. Thus, MpARK1 has the dual function in promoting rhizoid elongation and stabilizing growth polarity. This is reminiscent of the function of *Arabidopsis* ARK1 in root hairs[7,21]. ARK kinesin may play the evolutionarily conserved roles in tip growth of land plants. The recovery of *Arabidopsis ark* mutant by MpARK1 strongly supports this notion.

Although the origin of this plant-specific kinesin is not clear, it may be acquired after the colonization of terrestrial environments to efficiently promote the development of rooting structures.

How does MpARK1 execute the dual function? Our functional analysis strongly suggest that MpARK1 plays a pivotal role in organelle transport to enhance tip growth of rhizoids. In the absence of MpARK1, anterograde movement of the nucleus and plastids are significantly decreased, and localization of various organelles are shifted to the basal side of rhizoids, which may in turn severely affects cellular activity required for tip growth (e.g., allocation of RNAs, proteins, and metabolites, targeted secretion of various components to the apex). The association of MpARK1-Citrine with the nucleus and plastids is consistent with this. Further, Yosida et al. (co-submitted accompanying paper) also demonstrate that *P. patens* ARK kinesins drive organelle transport to promote tip growth. Therefore, ARK kinesins may drive anterograde transport of organelles to sustain tip growth in land plants.

We also found that MpARK1 participates in microtubule convergence at the tip to stabilize growth direction. Mp*ark1* mutant rhizoids exhibit no obvious microtubule foci due to dispersed growth direction of microtubule plus ends. Since MpARK1-Citrine moves toward the apex and accumulates at the apical microtubules, MpARK1 may direct microtubule growth and bundle microtubule plus ends at the apex like as another plant specific kinesins KINIDa/b in *P. patens* protonemata[6]. Alternatively, but not exclusively, MpARK1 may transport MpNEK1 to regulate the apical microtubule foci.

The roles of MpARK1 in organelle transport and microtubule organization might be mutually independent. Because of spatial separation between organelle transport (mainly at the shank region) and microtubule foci (at the apex), it is unlikely that MpARK1 regulates organelle transport through microtubule configuration. Another regulator of rhizoids, NIMA related kinase MpNEK1, localizes to microtubule foci and stabilizes growth direction by depolymerizing and reorganizing apical microtubules[35]. Mp*nek1* mutants show fluctuation of growth direction and defect of apical microtubules, but not abnormal organelle localization and transport. Thus, apical microtubule foci may not be required for organelle transport but rather stabilize direction of tip growth.

Previous studies have demonstrated that *Arabidopsis* ARK1 localizes to the growing plus-ends and promotes microtubule catastrophe during root hair elongation[7]. ARK1-mediated microtubule catastrophe is presumed to increase cytoplasmic free tubulin and growth velocity of microtubule plus ends. Our study indicates no obvious defects of Mp*ark1* mutants in microtubule dynamics, plus-end growth velocity and catastrophe. Thus, we inferred that the severe defects in rhizoid growth could not be attributed to microtubule dynamics but rather to obvious defects in organelle transport and microtubule convergence.

Recent studies demonstrate that kinesin-14 drives minus end-directed transport of organelles and cytoskeletons[10,11,14,15]. KCH drives retrograde transport of organelles in tip growing protomenata in *P. patens*[11], whereas ARK kinesins drive anterograde nuclear transport[9]. Although it remains unknown whether KCH functions in rhizoids, ARK and KCH may competitively function in organelle transport to coordinate intracellular organization. Because cell growth causes extensive

displacement and rearrangement of organelles, kinesin-mediated organelle relocation might be required to arrange intracellular structure for persistent tip growth and stable cellular activity.

Collectively, our results suggest that ARK corresponds to the predominant anterograde kinesins in animals (kinesin-1, 2, 3) which execute long-range transport of organelles[17]. ARK might be co-opted as a long-range transporter to enhance the persistent tip growth of rooting cells during land plant evolution. This coincides with the elongation of ER tubules along microtubules[38] and ARK1-mediated ER movement to the microtubule plus ends[25] in *Arabidopsis* and challenges the conventional view that actin-myosin-based transport is dominant in plants. In *Arabidopsis*, myosin XI-i promotes nuclear motility in the mature cells through interaction with nuclear membrane proteins WIT1/2[39], whereas rapid acropetal nuclear movement in growing root hairs could occur in the absence of myosin XI-i and microtubules are required for stable nuclear migration[40], suggesting that both actin- and microtubule-based motor proteins participate in this process. Although myosin function remains unclear in *M. polymorpha*, molecular activity of myosin XI is well conserved, but the velocity of organelle motility is very low compared with that in flowering plants[41]. Hence, actin-myosin system is not the main transport machinery in rhizoids. However, we could not exclude the possibility that ARK functions through actin-microtubule crosstalk and their regulators as shown in KCH[15,42], KCBP[43], and myosin VIII[44]. Further studies of plant kinesins, their cargos/interactors, and directional transport will reveal the fundamental mechanism of tip growth and transport systems in plants.

Methods

Plant Material and Growth Conditions

M. polymorpha accessions, Takaragaike-1 (Tak-1, male) and Tak-2 (female), were used as the wild-type. Thalli and gemmalings were grown at 22°C under continuous white light on the half-strength Gamborg's B5 medium [Gamborg's B5 medium mixed salt (Fujifilm Wako Pure chemical, Osaka, Japan), 0.5 g/L 2-morpholinoethanesulfonic acid (MES), 0.1 g/L myo-inositol, 0.001 g/L nicotinic acid, 0.001 g/L pyridoxine hydrochloride, 0.01 g/L thiamine hydrochloride, adjusted to pH 5.5 with KOH and solidified with 1% agar]. Antibiotics, claforan (100 mg/L), hygromycin (10 mg/L), and chlorsulfuron (5 μM) were added to the half B5 medium. For pharmacological analysis, oryzalin and latrunculin B were dissolved in dimethyl sulfoxide (DMSO) and added to B5 media as final concentrations of DMSO were less than 0.2%. Dormant gemmae were collected and plated on B5 media with or without drugs. Gametangiophore was induced under continuous white light with far-red irradiation as described previously[45]. *A. thaliana* Columbia accession was used as the wild type. The *ark1-1 ark2-1 ark3-1* triple mutant of *A. thaliana* were described previously[21]. Seeds of *A. thaliana* were germinated on the half-strength Murashige and Skoog (MS) agar medium and vertically incubated at 22°C under continuous white light as described previously[46].

Plasmid construction and transformation

For the mutagenesis of Mp*ARK1*, we generated CRISPR/Cas9 constructs. Two complementary

DNA oligos encoding 20-base target sequences of gRNA (Table S1) were annealed and cloned into the *Bsa*I site of an entry vector pMpEn_03 according to ref. 47. The Mp*U6-1pro:gRNA* sequences in pMpEn_03 plasmids were transferred into a binary vector pMpGE010[47] by LR reaction using Gateway LR Clonase II enzyme mix (Thermo Fisher Scientific, Tokyo, Japan). The resulting binary vectors were introduced into *Agrobacterium* GV3101 (pMP90) strain by electroporation. The constructs were introduced into wild type F1 sporelings derived from sexual crosses between Tak-2 and Tak-1 by *Agrobacterium*-mediated transformation method[34]. Transformants were selected on the half B5 agar medium containing 10 μg/ml hygromycin B and 100 μg/ml cefotaxime. For the selection of mutants, genomic DNA of transformants was extracted and subjected to PCR by a DNA polymerase KOD FX neo (Toyobo) and gene specific primers to amplify DNA regions flanking the target sequences. The primers used for PCR are shown in Table S1. By using amplified DNA as a template, sequence reaction was performed by BigDye terminator ver.3.1 (Thermo Fisher Scientific) and a gene-specific primer (Table S1). DNA sequencing was performed by ABI3500 Genetic Analyzer (Thermo Fisher Scientific).

To construct Mp*ARK1pro:*Mp*ARK1-Citrine*, the full-length MpARK1 was amplified from Tak-1 cDNA by PCR using KOD plus (TOYOBO) with the primers in Table S1 and cloned into pENTR/D-TOPO cloning vector (Thermo Fisher Scientific). This vector was confirmed by sequencing and designated as pENTR/D-TOPO-MpARK1. The Mp*ARK1* promoter region, including a 3.4-kb region upstream of the initiation codon, was amplified from Tak-1 genomic DNA by PCR using KOD plus with the primers in Table S1 and cloned into the unique *Not*I site of pENTR/D-TOPO-MpARK1 by In-Fusion system (Takara) to generate pENTR/D-TOPO-MpARK1pro:MpARK1. To introduce a silent synonymous mutation for complementation of Mp*ark1-g1* mutants, the PAM sequence of gRNA1 was mutagenized by KOD mutagenesis kit (Toyobo) and primers shown in Table S1. The resulting entry vector was used in the LR reaction with the Gateway binary vector pMpGWB307[35] to generate Mp*ARK1pro:*Mp*ARK1-Citrine* construct. This was introduced into regenerating thalli of the Mp*ark1-g1* mutants by the method described in ref. 48. Transformants were selected on the B5 medium containing 0.5 μM chlorsulfuron and 100 μg/ml cefotaxime.

To generate a rigor mutation (T172N), pENTR/D-TOPO-MpARK1pro:MpARK1 with a mutation in the PAM sequence was subjected to inverse PCR using KOD mutagenesis kit (Toyobo) and primers shown in Table S1. To remove the armadillo repeats, ENTR/D-TOPO-MpARK1pro:MpARK1 with a PAM mutation was subjected to inverse PCR using KOD mutagenesis kit (Toyobo) and primers shown in Table S1. The resulting entry vectors were subjected to the LR reaction with the Gateway binary vector pMpGWB307[35] to generate Mp*ARK1pro:*Mp*ARK1*^{T172N}*-Citrine* and Mp*ARK1pro:*Mp*ARK1*^{dARM}*-Citrine* constructs. These were introduced into regenerating thalli of the Mp*ark1-g1* mutants by the method described in ref. 48. Transformants were selected on the B5 medium containing 0.5 μM chlorsulfuron and 100 μg/ml cefotaxime.

To construct Mp*ARK1pro:Citrine-NLS*, a part of MpARK1 cDNA spanning from the 21st amino acid (Arg21) to the 883rd amino acid (Tyr883) in pENTR/D-TOPO-MpARK1pro:MpARK1 was

removed by inverse PCR using KOD mutagenesis kit (Toyobo) and primers shown in Table S1. The resulting entry vector, including a 3.4-kb region upstream of the initiation codon and 60-b coding region corresponding to the 20-amino-acid sequence of MpARK1, was subjected to the LR reaction with the Gateway binary vector pMpGWB115[35] to generate Mp*ARK1pro:Citrine-NLS* construct, in which Citrine-NLS was translationally fused with the first 20-amino-acid sequence of MpARK1. Mp*ARK1pro:Citrine-NLS* construct was introduced into wild type F1 sporelings as previously described[34]. Transformants were selected with 10 µg/ml hygromycin B and 100 µg/ml cefotaxime.

To construct *CaMV35Spro:*Mp*EB1a-Citrine*, Mp*EB1a* genomic CDS was amplified from Tak-1 genomic DNA by PCR using KOD plus with the primers in Table S1 and cloned into pENTR/D-TOPO. This entry vector was used in the LR reaction with the Gateway binary vector pMpGWB306[35] to generate *CaMV35Spro:*Mp*EB1a-Citrine* construct, in which Citrine was translationally fused with MpEB1b. *CaMV35Spro:*Mp*EB1a-Citrine* was introduced into F1 wild-type sporelings derived from crosses between Tak-1 and Tak-2 or into regenerating thalli of Mp*ARK1* mutants as described above. Transformants were selected with 0.5 µM chlorsulfuron and 100 µg/ml cefotaxime.

CaMV35Spro:Citrine-Mp*TUB2* was constructed by LR reaction between pENTR/D-TOPO-MpTUB2[36] and pMpGWB305[35]. *CaMV35Spro:Citrine*-Mp*TUB2* was introduced into F1 wild-type sporelings derived from crosses between Tak-1 and Tak-2 or into regenerating thalli of Mp*ARK1* mutants as described above. Transformants were selected with 0.5 µM chlorsulfuron and 100 µg/ml cefotaxime.

To construct Mp*ARK1pro:*Mp*ARK1-TagRFP*, pENTR/D-TOPO-MpARK1pro:MpARK1 (with a silent mutation in the PAM sequence of gRNA1) was used in the LR reaction with the Gateway binary vector pMpGWB326[35] to generate Mp*ARK1pro:*Mp*ARK1-TagRFP* construct. This was introduced into regenerating thalli of *CaMV35Spro:Citrine*-Mp*TUB2*[36] (pMpGWB106-Mp*TUB2*) or *CaMV35Spro:*Mp*EB1a-Citrine* by the method described above. Transformants were selected on the B5 medium containing 0.5 µM chlorsulfuron and 100 µg/ml cefotaxime.

To visualize nuclear movement, Mp*NEK1pro:Citrine-NLS* was constructed by LR reaction between pENTR/D-TOPO-Mp*NEK1pro*[36] and pMpGWB315[35]. Mp*NEK1pro:Citrine-NLS* construct was introduced into F1 wild-type sporelings derived from crosses between Tak-1 and Tak-2 or into regenerating thalli of Mp*ARK1* mutants as described above. Transformants were selected on the B5 medium containing 0.5 µM chlorsulfuron and 100 µg/ml cefotaxime.

For the localization analysis of MpNEK1, pMpGWB307-Mp*NEK1pro:*Mp*NEK1*[36] was introduced into F1 wild-type sporelings derived from crosses between Tak-1 and Tak-2 or into regenerating thalli of Mp*ARK1* mutants as described above. Transformants were selected on the B5 medium containing 0.5 µM chlorsulfuron and 100 µg/ml cefotaxime.

To construct At*NEK6pro:*Mp*ARK1-GFP*, pENTR/D-TOPO-MpARK1 was used in the LR reaction with the Gateway binary vector pGWB504[49] containing *NEK6* promoter (details of this construct will be described elsewhere by H.M.) to generate At*NEK6pro:*Mp*ARK1-GFP* construct. This was introduced into *ark1-1 ark2-1 ark3-1* triple mutant[21] of *A. thaliana* by floral dip method[50].

Transformants were selected on the MS medium containing 10 µg/ml hygromycin B and 100 µg/ml cefotaxime.

Microscopy

Plants were observed and photographed by a stereomicroscope S8 Apo (Leica Microsystems, Wetzlar, Germany) equipped with a CCD camera EC3 (Leica Microsystems) or by a single-lens reflex camera D5600 (Nikon, Tokyo, Japan). Morphology of rhizoids was observed by S8 Apo equipped with EC3 or a light microscope DM5000B (Leica) equipped with a CCD camera DFC500 (Leica). Rhizoid length was quantified by ImageJ software (NIH, USA).

For live imaging of rhizoids, the B5 agar medium was poured and solidified in a glass bottom dish (35 mm in diameter x 10 mm in thickness). The central part of the medium on the bottom slide glass was removed by tweezers and was supplied with about 200 µL of melted B5 agar medium to form a thin solidified medium. The gemmi were planted on the center of medium and grown for 2-7 days under continuous white light at 22°C. The details of this method will be described elsewhere by A.K. and H.M. The gemmaling was observed under a FV1200 confocal laser-scanning microscope (Olympus) equipped with a high-sensitivity GaAsP detector and silicone oil objective lenses (30x and 60x, Olympus). Silicone oil (SIL300CS, Olympus) was used as immersion media for objective lens. The images were analyzed by ImageJ (National Institutes of Health, USA) and LPixel ImageJ plugins (LPixel, Japan).

RT-qPCR

Total RNA was isolated by NucleoSpin® RNA Plant RNA isolation kit (Takara Bio, Kusatsu, Japan) according to the manufacture's instruction. RNA was quantified with a spectrophotometer DU730 (Beckman Coulter, CA, USA). Reverse transcription was performed with 0.5 µg of total RNA of each sample by ReverTra Ace reverse transcriptase (Toyobo, Osaka, Japan) according to the manufacture protocol. Quantitative real-time PCR was performed in Thermal Cycler Dice Real Time System Lite (Takara Bio) using KOD SYBR qPCR Mix (Toyobo) and gene-specific primers shown in Table S1. Transcript levels of Mp*ACT* were used as references for normalization[51]. RT-qPCR was conducted in four biological replicates.

Phylogenetic analysis

For phylogenetic analysis of ARK kinesins, we used a conserved motor domain at the N-terminus. Sequence information was collected in Phytozome (http://phytozome.jgi.doe.gov/pz). To generate a maximum-likelihood bootstrap consensus tree, the sequences were aligned by MUSCLE[52] and phylogenetic analyses were conducted in MEGA7[53]. The evolutionary history was estimated using the Maximum Likelihood method based on the JTT matrix-based model. The bootstrap consensus tree deduced from 1000 replicates is adopted to represent the evolutionary history of the proteins analyzed. The percentages of replicate trees in which the associated sequences clustered together are shown next to the branches. The branch lengths were measured in the number of substitutions per site.

Statistical analyses

All statistical analyses were conducted using R software (R 3.6.3, R Foundation for Statistical Computing, Vienna, Austria). Tukey's HSD test was used for comparisons of multiple sample means. The types of statistical tests, sample sizes, and significance level (*P* value) are shown in figure legend.

Acknowledgements

We thank Drs. Shigeo Sugano, Keishi Osakabe, and Takayuki Kohchi for providing CRISPR/Cas9 vectors, Drs. Ryuichi Nishihama, Kimitsune Ishizaki, and Takayuki Kohchi for the early Mp*ARK1* sequence, pMpGWBs and MpTUB2 constructs, Dr. Tatsuya Sakai for *Arabidopsis ark* mutant seeds, Dr. Tsuyoshi Nakagawa for pGWB504, and Dr. Gohta Goshima for discussing and sharing unpublished results. This work was supported by Grants-in-Aid from the JSPS (JSPS KAKENHI Grant Numbers 16K07403, 19K06709, and 21H00370 to H.M.), Ryobi Teien Memory Foundation, and Naito Foundation to H.M.

References

1. Rounds, C. M. & Bezanilla, M. (2013) Growth mechanisms in tip-growing plant cells. Annu. Rev. Plant Biol. 64, 243-265.
2. Orr, R., Cheng, X., Vidali, L. & Bezanilla, M. (2020) Orchestrating cell morphology from the inside out – using polarized cell expansion in plants as a model. Curr.Opin. Cell Biol. 62, 46-53.
3. Denninger, P., Reichelt, A., Schmidt, V. A. F., Mehlhorn, D. G., Asseck, L. Y., Stanley, C. E., Keinath, N. F., Evers, J.-F., Grefen, C. & Grossmann, G. (2019) Distinct RopGEFs successively drive polarization and outgrowth of root hairs. Curr. Biol. 29, 1854-1865.
4. Cheng, X., Mwaura, B. W., Stauffer, S. R. C. & Bezanilla, M. (2020) A fully functional ROP fluorescent fusion protein reveals roles for this GTPase in subcellular and tissue-level patterning. Plant Cell 32: 3436–3451.
5. Shimmen, T. & Yokota, E. (2004) Cytoplasmic streaming in plants. Curr. Opin. Cell Biol. 16, 68-72.
6. Tominaga, M. & Ito, K. (2015) The molecular mechanism and physiological role of cytoplasmic streaming. Curr. Opin. Plant Biol. 27, 104-110.
7. Eng, R. C., & Wasteneys, G. O. (2014) The microtubule plus-end tracking protein ARMADILLO-REPEAT KINESIN1 promotes microtubule catastrophe in Arabidopsis. Plant Cell 26, 3372-3386.
8. Hiwatashi, Y., Sato, Y. & Doonan, J. H. (2014) Kinesins have a dual function in organizing microtubules during both tip growth and cytokinesis in *Physcomitrella patens*. Plant Cell 26,1256-1266.
9. Miki, T., Nishina, M. & Goshima, G. (2015) RNAi screening identifies the armadillo repeat-containing kinesins responsible for microtubule-dependent nuclear positioning in

Physcomitrella patens. Plant Cell physiol. 56, 737-749.

10. Yamada, M., Tanaka-Takiguchi, Y., Hayashi, M., Nishina, M. & Goshima, G. (2017) Multiple kinesin-14 family members drive microtubule minus end-directed transport in plant cells. J. Cell Biol. 216, 1705-1714.
11. Yamada, M. & Goshima, G. (2018) The KCH kinesin drives nuclear transport and cytoskeletal coalescence to promote tip cell growth in *Physcomitrella patens*. Plant Cell **30,** 1496-1510.
12. Leong, S. Y., Edzuka, T., Goshima, G. & Yamada, M. (2020) Kinesin-13 and Kinesin-8 function during cell growth and division in the moss *Physcomitrella patens*. Plant Cell 32, 683-702.
13. Nebenführ, A. & Dixit, R. (2018) Kinesins and myosins: molecular motors that coordinate cellular functions in plants. Ann. Rev. Plant Biol. 69, 329-361.
14. Jonsson, E., Yamada, M., Vale, R. D. & Goshima, G. (2015) Clustering of a kinesin-14 motor enables processive retrograde microtubule-based transport in plants. Nat. Plants 1, 15087.
15. Walter, W. J., Machens, I., Rafieian, F. & Diez, S. (2015) The non-processive rice kinesin-14 OsKCH1 transports actin filaments along microtubules with two distinct velocities. Nat. Plants 1, 15111.
16. Yoshida, M. W., Yamada, M. & Goshima, G. (2019) Moss kinesin-14 KCBP accelerates chromatid motility in anaphase. Cell Struct. Func. 44, 95-104.
17. Hirokawa, N., Niwa, S. & Tanaka, Y. (2010) Molecular motors in neurons: transport mechanisms and roles in brain function, development, and disease. Neuron 68, 610-638.
18. Reddy, A. S. & Day, I. S. (2001) Kinesins in the *Arabidopsis* genome: a comparative analysis among eukaryotes. BMC Genomics 2, 2.
19. Shen, Z., Collatos, A. R., Bibeau, J. P., Furt, F. & Vidali, L. (2012) Phylogenetic analysis of the Kinesin superfamily from *Physcomitrella*. Front. Plant Sci. 3, 230.
20. Jones, M. A., Raymond, M. J. & Smirnoff, N. (2006) Analysis of the root-hair morphogenesis transcriptome reveals the molecular identity of six genes with roles in root-hair development in *Arabidopsis*. Plant J. 45: 83–100.
21. Sakai, T., Honing, H., Nishioka, M., Uehara, Y., Takahashi, M., Fujisawa, N., Saji, K., Seki, M., Shinozaki, K., Jones, M. A., Smirnoff, N., Okada, K. & Wasteneys, G. O. (2008) Armadillo repeat-containing kinesins and a NIMA-related kinase are required for epidermal-cell morphogenesis in *Arabidopsis*. Plant J. 53, 157-171.
22. Eng, R. C., Halat, L. S., Livingston, S. J., Sakai, T., Motose, H. & Wasteneys, G. O. (2017) The ARM domain of ARMADILLO-REPEAT KINESIN 1 is not required for microtubule catastrophe but can negatively regulate NIMA-RELATED KINASE 6 in *Arabidopsis thaliana*. Plant Cell Physiol. 58, 1350–1363.
23. Yang, G., Gao, P., Zhang, H., Huang, S. & Zheng, Z.L. (2007) A mutation in MRH2 kinesin enhances the root hair tip growth defect caused by constitutively activated ROP2 small GTPase in *Arabidopsis*. PLoS One 2: e1074.
24. Yoo, C. M. & Blancaflor, E. B. (2013) Overlapping and divergent signaling pathways for ARK1 and AGD1 in the control of root hair polarity in *Arabidopsis thaliana*. Front. Plant Sci.

4: 528.

25. Sun, J., Zhang, M., Qi, X., Doyle, C. & Zheng, H. (2020) Armadillo-repeat kinesin1 interacts with *Arabidopsis* atlastin RHD3 to move ER with plus-end of microtubules. Nat. Comm. 11:5510.
26. Malcos, J. L. & Cyr, R. J. (2011) An ungrouped plant kinesin accumulates at the preprophase band in a cell cycle-dependent manner. Cytoskeleton 68, 247-258.
27. Lau, O. S., Davies, K. A., Chang, J., Adrian, J., Rowe, M. H., Ballenger, C. E. & Bergmann, D. C. (2014) Direct roles of SPEECHLESS in the specification of stomatal self-renewing cells. Science 345, 1605-1609.
28. Jones, V. A. & Dolan, L. (2012）The evolution of root hairs and rhizoids. Ann Bot.110, 205-212.
29. Hetherington, A. J. & Dolan, L. (2017) Bilaterally symmetric axes with rhizoids composed the rooting structure of the common ancestor of vascular plants. Phil. Trans. R. Soc. B 373, 20170042.
30. Proust, H., Honkanen, S., Jones, V. A. S., Morieri, G., Prescott, H., Kelly, S., Ishizaki, K., Kohchi, T. & Dolan, L (2016) RSL Class I genes controlled the development of epidermal structures in the common ancestor of land plants. Curr. Biol. 26, 93-99.
31. Honkanen, S., Jones, V. A. S., Morieri, G., Champion, C., Hetherington, A. J., Kelly, S., Proust, H., Saint-Marcoux, D., Prescott, H. & Dolan, L (2016) The mechanism forming the cell surface of tip-growing rooting cells is conserved among land plants. Curr. Biol. 26, 3238–3244.
32. Breuninger, H., Thamm, A., Streubel, S., Sakayama, H., Nishiyama, T. & Dolan, L. (2016). Diversification of a bHLH transcription factor family in streptophytes led to the evolution of antagonistically acting genes controlling root hair growth. Curr. Biol. 26, 920–934.
33. Bowman, J. L. et al. (2017) Insights into land plant evolution garnered from the *Marchantia polymorpha* genome. Cell 171: 287-304.
34. Ishizaki, K., Chiyoda, S., Yamato, K. T. & Kohchi, T. (2008) Agrobacterium-mediated transformation of the haploid liverwort *Marchantia polymorpha* L., an emerging model for plant biology. Plant Cell Physiol. 49, 1084-1091.
35. Ishizaki, K., Nishihama, R., Ueda, M., Inoue, K., Ishida, S., Nishimura, Y., Shikanai, T. & Kohchi, T. (2015) Development of gateway binary vector series with four different selection markers for the liverwort *Marchantia polymorpha*. PLoS One 10, e0138876.
36. Otani, K., Ishizaki, K., Nishihama, R., Takatani, S., Kohchi, T., Takahashi, T. & Motose, H. (2018) An evolutionarily conserved NIMA-related kinase directs rhizoid tip growth in the basal land plant *Marchantia polymorpha*. Development 145, pii: dev154617.
37. Champion, C., Lamers, J., Jones, V. A. S., Morieri, G., Honkanen, S. & Dolan, L. (2021) Microtubule associated protein WAVE DAMPENED2-LIKE (WDL) controls microtubule bundling and the stability of the site of tip-growth in *Marchantia polymorpha* rhizoids. PLoS Genet. 17, e1009533.
38. Hamada, T., Ueda, H., Kawase, T. & Hara-Nishimura, I. (2014) Microtubules contribute to tubule elongation and anchoring of endoplasmic reticulum, resulting in high network

complexity in Arabidopsis. Plant Physiol. 166, 1869–1876.

39. Tamura, K., Iwabuchi, K., Fukao, Y., Kondo, M., Okamoto, K., Ueda, H., Nishimura, M. & Hara-Nishimura, I. (2013) Myosin XI-i links the nuclear membrane to the cytoskeleton to control nuclear movement and shape in Arabidopsis. Curr. Biol. 23, 1776-1781.
40. Brueggeman, J. M., Windham, I. A. & Nebenführ, A. (2022) Nuclear movement in growing Arabidopsis root hairs involves both actin filaments and microtubules. J. Exp.Bot., erac207.
41. Duan, Z., Tanaka, M., Kanazawa, T., Haraguchi, T., Takyu, A., Era, A., Ueda, T., Ito, K. & Tominaga, M. (2020) Characterization of ancestral myosin XI from *Marchantia polymorpha* by heterologous expression in *Arabidopsis thaliana*. Plant J. 104, 460-473.
42. Li, Y., et al. (2021) A minus-end directed kinesin motor directs gravitropism in *Physcomitrella patens*. Nat. Comm. 12, 4470.
43. Tian, J., Han, L., Feng, Z., Wang, G., Liu, W., Ma, Y., Yu, Y. & Kong, Z. (2015) Orchestration of microtubules and the actin cytoskeleton in trichome cell shape determination by a plant-unique kinesin. eLife, 4, e09351.
44. Wu, S.-Z. & Bezanilla, M. (2018) Actin and microtubule cross talk mediates persistent polarized growth. J. Cell Biol. 217, 3531-3544.
45. Chiyoda, S., Ishizaki, K., Kataoka, H., Yamato, K. T. & Kohchi, T. (2008) Direct transformation of the liverwort Marchantia polymorpha L. by particle bombardment using immature thalli developing from spores. Plant Cell Rep. 27, 1467-1473.
46. Takatani, S., Verger, S., Okamoto, T., Takahashi, T., Hamant, O. & Motose, H. (2020) Microtubule response to tensile stress is curbed by NEK6 to buffer growth variation in the *Arabidopsis* hypocotyl. Curr. Biol. 30, 1491-1503.
47. Sugano, S. S., Nishihama, R., Shirakawa, M., Takagi, J., Matsuda, Y., Ishida, S., Shimada, T., Hara-Nishimura, I., Osakabe, K. & Kohchi, T. (2018) Efficient CRISPR/Cas9-based genome editingand its application to conditional genetic analysis in *Marchantia polymorpha*. PLoS One 13, e0205117.
48. Kubota, A., Ishizaki, K., Hosaka, M. & Kohchi, T. (2013) Efficient *Agrobacterium*-mediated transformation of the liverwort *Marchantia polymorpha* using regenerating thalli. Biosci. Biotechnol. Biochem. 77, 167-172.
49. Nakagawa, T. et al. (2009) Improved Gateway binary vectors: high-performance vectors for creation of fusion constructs in transgenic analysis of plants. Biosci. Biotechnol. Biochem. 71, 2095-2100.
50. Clough, S. J. & Bent, A. F. (1998) Floral dip: a simplified method for *Agrobacterium*-mediated transformation of *Arabidopsis thaliana*. Plant J. 16, 735-743.
51. Saint-Marcoux, D., Proust, H., Dolan, L. & Langdale, J. A. (2015) Identification of reference genes for real-time quantitative PCR experiments in the liverwort Marchantia polymorpha. PLoS One 10, e0118678.
52. Edgar, R. C. (2004) MUSCLE: multiple sequence alignment with high accuracy and high throughput. Nuc. Acid. Res. 32, 1792–1797.
53. Kumar, S., Stecher, G., & Tamura, K. (2016) MEGA7: Molecular Evolutionary Genetics

Analysis Version 7.0 for bigger datasets. Mol. Biol. Evol. 33, 1870-1874.

Figure legend

Fig. 1. Phylogeny, structure, and expression of Mp*ARK1*.

(a) Phylogenetic tree of ARK family. A maximum-likelihood bootstrap tree based on the conserved motor domain. The numbers on the branches show bootstrap values calculated from 1000 replicates. Amtr: *Amborella trichopoda*, At: *Arabidopsis thaliana*, Mp: *Marchantia polymorpha*, Os: *Oryza sativa*, Pp: *Physcomitrium patens*, Sm: *Selaginella moellendorffii*.

(b) Protein structures of MpARK1 and AtARK1-3.

(c) The expression pattern of Mp*ARK1pro:Citrine-NLS*. Left panel: a confocal image of Citrine-NLS (green) in the rhizoid nucleus, right panel: confocal z-stack image of Citrine-NLS (green) in the nuclei of thallus cells, especially in air pore cells (arrows).

Fig. 2. Mp*ARK1* is required for tip growth of rhizoids.

(a) Exon-intron structure of MpARK1. Box, exon; line, intron; grey, 5' or 3' untranslated region; magenta, motor domain; blue, coiled-coil domain; yellow, armadillo repeats.

(b) Morphology of 14-day-old wild type (Tak-1) and Mp*ark1* mutants (Mp*ark1-g1* and Mp*ark1-g2*). Lower panels are images of rhizoids. Arrowheads indicate rhizoids.

(c) Structure of MpARK1 constructs introduced into the Mp*ark1-g1* mutant.

(d) Morphology of 14-day-old Mp*ark1-g1* introduced with the full length MpARK1-Citrine, MpARK1-Citrine without armadillo repeats (dARM), or rigor mutant MpARK1-Citrine (Rigor) under the control of Mp*ARK1* promoter. Lower panels show rhizoid morphology.

(e) Growth velocity of rhizoids in the wild type (Tak-1), Mp*ark1-g1*, and Mp*ark1-g1* complemented with the full length MpARK1-Citrine (Mp*ARK1pro:*Mp*ARK1-Citrine*). Values are shown by box plots (n=7). The different letters indicate significant differences by Tukey's HSD test ($P < 0.05$).

Fig. 3. MpARK1 localizes in microtubule foci at the rhizoid apex.

(a) Subcellular localization of MpARK1-Citrine. Confocal z-stack image and orthogonal planes of a rhizoid of the complemented line (Mp*ark1-g1* mutant with Mp*ARK1pro:*Mp*ARK1-Citrine*).

(b) Subcellular localization of full length MpARK1-Citrine and armadillo-repeats-deleted MpARK1-Citrine (dARM). A single optical section of a rhizoid in Mp*ark1-g1* introduced with the full length MpARK1-Citrine and MpARK1 dARM-Citrine.

(c) Localization of MpARK1-TagRFP to the apical microtubules. Confocal z-stack image of double labelled line (Mp*ARK1pro:*Mp*ARK1-TagRFP, CaMV35Spro:Citrine*-Mp*TUB2*). Arrows and a bracket indicate localization of MpARK1-TagRFP in the microtubule ends and the side of microtubule, respectively.

(d) Different localization of MpARK1-TagRFP and MpEB1a-Citrine (microtubule plus ends). Confocal z-stack image of double labelled line (Mp*ARK1pro:*Mp*ARK1-TagRFP*,

CaMV35Spro:MpEB1a-Citrine).

Fig. 4. MpARK1 is required for microtubule convergence at the rhizoid apex.

(a) Microtubules labeled with Citrine-MpTUB2 in the wild type and Mp*ark1-g1*.

(b) The growing plus ends of microtubules labeled with MpEB1a-Citrine in the wild type and Mp*ark1-g1*.

(c) Quantification of fluorescent density of MpEB1a-Citrine signal at the apical and basal regions of rhizoids in the wild type and Mp*ark1-g1*. The apical region is 0-10 µm region away from the rhizoid apex and the basal region is 50-100 µm shank region away from the apex. Values are shown by box plots (*n*=10 cells). The different letters indicate significant differences by Tukey's HSD test ($P < 0.04$).

(d) Ratio of MpEB1a-Citrine signal at the apical and basal regions of rhizoids in the wild type and Mp*ark1-g1*. Values are shown by box plots (*n*=10 cells). An asterisk indicates significant difference from the value of the wild type (Wilcoxon rank sum test, $P < 0.001$).

(e) Direction of movement of MpEB1a-Citrine comets. The angle indicates a deviation from the longitudinal axis of rhizoid. Values are shown by box plots (*n*=100 comets, 5 cells). An asterisk indicates significant difference from the value of the wild type (Wilcoxon rank sum test, $P < 0.03$).

(f) Proportions of MpEB1a-Citrine comets moving toward the apex or the base (*n*=100 comets, 5 cells).

(g) Velocity of MpEB1a-Citrine comets. Values are shown by box plots (wild type *n*=151, 8 cells, Mp*ark1 n*=155, 9 cells, Wilcoxon rank sum test, $P > 0.05$).

(h) Catastrophe of microtubule plus ends. The catastrophe of the plus ends was evaluated by the reciprocal of MpEB1a-Citrine comet duration time (time from appearance to disappearance of EB1 comet). Values are shown by box plots (*n*=80, 5 cells, Wilcoxon rank sum test, $P > 0.05$).

Fig. 5. MpARK1 is required for organelle transport in rhizoids.

(a) Localization of the nucleus and plastids in rhizoids of the wild type and Mp*ark1-g1*.

(b, c) Velocity of nuclear movement (b) and distance between the nucleus and the rhizoid apex (c) in the wild type and Mp*ark1-g1*. The movement of nuclei labelled with Citrine-NLS (Mp*NEK1pro:Citrine-NLS*) was observed in a confocal microscope. Values are shown by box plots (*n*=20 nuclei in (b), *n*=25 nuclei in (c)). An asterisk indicates significant difference from the value of the wild type (Wilcoxon rank sum test, $P < 0.01$).

(d, e) Velocity of plastid movement (d) and distance between plastids and the rhizoid apex (e) in the wild type and Mp*ark1-g1*. Five plastids were analyzed in each cell (*n*=6 cells). The five plastids nearest to the apex were measured in (e). Values are shown by box plots (*n*=30 plastids). An asterisk indicates significant difference from the value of the wild type (Wilcoxon rank sum test, $P < 0.01$).

Fig. 6. MpARK1-mediated rhizoid growth is required for soil holding and reproductive development.

(a, b) Thallus growth (a) and soil-holding capacity (b) of the wild type, Mp*ark1-g1*, Mp*ark1-g2*, and Mp*ark1-g1* with the full length MpARK1-Citrine, armadillo-repeats-deleted MpARK1-Citrine (dARM), or rigor mutant MpARK1-Citrine (Rigor). Plants were grown on the soil for one month.
(c) Morphology of male reproductive organs (antheridiophores) of the wild type, Mp*ark1-g1*, Mp*ark1-g2*, and Mp*ark1-g1* with the full length MpARK1-Citrine (Full length), armadillo-repeats-deleted MpARK1-Citrine (dARM), or rigor mutant MpARK1-Citrine (Rigor).

Fig. S1. Phenotype and genotype of Mp*ark1* mutants.
(a) RT-qPCR analysis of Mp*ARK1*. Total RNA was isolated from the 21-day-old wild type plants and subjected to RT-qPCR analysis using two primer sets shown in the upper diagram. Columns and error bars indicate mean values and standard deviations of n=4, respectively. Asterisk indicates significant difference (Wilcoxon rank sum test, $P < 0.03$).
(b) Morphology of the wild type and Mp*ark1-g1* mutants (upper panels: 7-day-old plants, middle and lower panels: 21-day-old plants). Arrows indicate rhizoids.
(c, d) Genomic sequences flanking target sites of MpARK1 (c, gRNA1; d, gRNA2). DNA and amino acid sequences of the wild type (WT) and mutant lines. Deleted bases are shown by hyphens. Inserted or substituted sequences are colored in red. Open box: PAM sequence.

Fig. S2. Localization and dynamics of MpARK1-Citrine.
(a) Dynamics of MpARK1-Citrine in the rhizoid apex. Mp*ark1-g1* complemented with the full length MpARK1-Citrine was observed in a confocal microscope. This corresponds to the right cell in Movie 1.
(b) Velocity of MpARK1-Citrine particles moving acropetally (apical) or basipetally (basal). Columns and error bars indicate mean values and standard deviations, respectively [n=6 cells both in apical direction (n=119 particles) and basal direction (n=60 particles)].
(c) Co-localization of MpARK1-TagRFP and Citrine-MpTUB2 (microtubules). Confocal z-stack image of double labelled line (Mp*ARK1pro:*Mp*ARK1-TagRFP, CaMV35Spro:Citrine*-Mp*TUB2*).
(d) Distinct localization of MpARK1-TagRFP and MpEB1a-Citrine (microtubule plus ends). Left panels, single cortical image in the apical cortical region of a rhizoid of double labelled line (Mp*ARK1pro:*Mp*ARK1-TagRFP, CaMV35Spro:* Mp*EB1a-Citrine*). Right panels, fluorescence intensity profile of MpEB1a-Citrine (upper) and MpARK1-TagRFP (lower) along the yellow dashed line in the upper left panel.
(e) Effects of oryzalin and latrunculin B (LatB) on the localization of MpARK1-Citrine. Mp*ark1-g1* complemented with Mp*ARK1pro:*Mp*ARK1-Citrine* was treated with 10 µM oryzalin or 1 µM latrunculin B for 15 min and observed under a confocal microscope. Arrows indicate MpARK1-Citrine.

Fig. S3. Localization of MpNEK1-Ctrine in the wild type and Mp*ark1-g1* mutant.
Confocal z-stack image of MpNEK1-Ctrine (Mp*NEK1pro:*Mp*NEK1-Citrine*) in the wild type and Mp*ark1-g1* mutant.

Fig. S4. MpARK1 participates in organelle transport.
(a, b) Association of MpARK1-Citrine with plastids (a) and the nucleus (b).
(c) Localization of mitochondria, vacuoles, and vesicles in rhizoids of the wild type and Mp*ark1-g1*, stained by DiOC6, MDY-64, and BODIPY-BFA, respectively. The wild type and Mp*ark1-g1* were stained with 1 µg/mL DiOC6, 1 µM MDY-64, or 0.5 µM BODIPY-BFA for 5 min and observed under a confocal microscope.

Fig. S5. MpARK1 rescues the growth defect of root hairs in *Arabidopsis ark1 ark2 ark3* mutant.
The roots of the wild type and *ark1-1 ark2-1 ark3-1* mutant (*ark123*) with or without At*NEK6pro:*Mp*ARK1-Citrine* were observed in a stereomicroscope.

Movie 1. Dynamics of MpARK1-Citrine in the apical dome of rhizoids. Time-lapse of rhizoids of Mp*ark1-g1* complemented with Mp*ARK1pro:*Mp*ARK1-Citrine*. Images were acquired every 6 seconds (25 fps).

Movie 2. Dynamics of MpARK1-Citrine in a rhizoid. Time-lapse of a rhizoid of Mp*ark1-g1* complemented with Mp*ARK1pro:*Mp*ARK1-Citrine*. Images were acquired every 5 seconds (25 fps).

Movie 3. Dynamics of MpEB1a-Citrine in the wild-type rhizoids. Time-lapse of rhizoids of the wild type with *CaMV35Spro:*Mp*EB1a-Citrine*. Images were acquired every 5 seconds (20 fps).

Movie 4. Dynamics of MpEB1a-Citrine in the Mp*ark1-g1* rhizoid. Time-lapse of a rhizoid of the Mp*ark1-g1* mutant with *CaMV35Spro:*Mp*EB1a-Citrine*. Images were acquired every 4 seconds (20 fps).

Movie 5. Motility of the nucleus (green) and plastids (magenta) in the wild-type rhizoid. Time-lapse of a rhizoid of the wild type with Mp*NEK1pro:Citrine-NLS*. Images were acquired every 8 seconds (20 fps).

Movie 6. Motility of the nucleus (green) and plastids (magenta) in the Mp*ark1-g1* mutant rhizoid. Time-lapse of a rhizoid of the Mp*ark1-g1* mutant with Mp*NEK1pro:Citrine-NLS*. Images were acquired every 15 seconds (10 fps).

Fig. 1

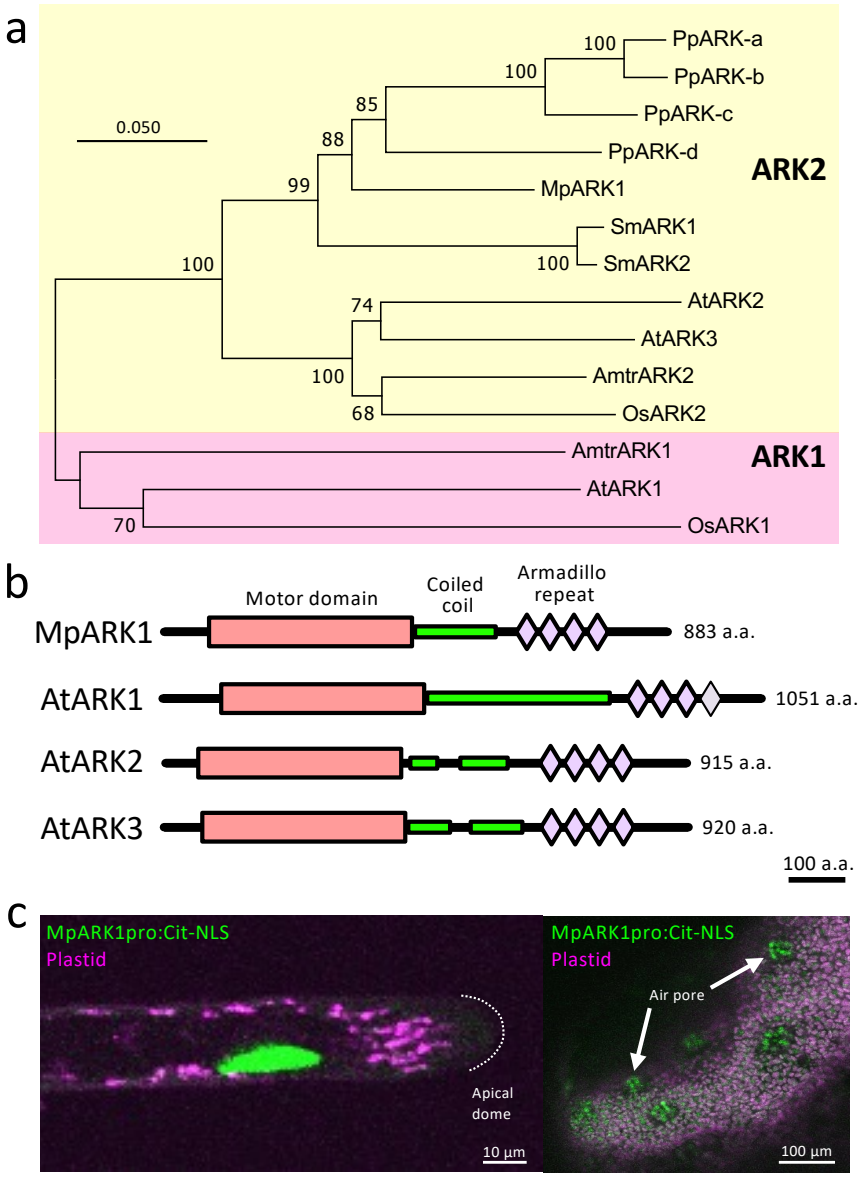
a
0.050
PpARK-a
PpARK-b
PpARK-c
PpARK-d
MpARK1
SmARK1
SmARK2
AtARK2
AtARK3
AmtrARK2
OsARK2
AmtrARK1
AtARK1
OsARK1
ARK2
ARK1
100
100
85
88
99
100
100
74
100
68
70
b
Motor domain
Coiled coil
Armadillo repeat
MpARK1
883 a.a.
AtARK1
1051 a.a.
AtARK2
915 a.a.
AtARK3
920 a.a.
100 a.a.
c
MpARK1pro:Cit-NLS
Plastid
Apical dome
10 µm
MpARK1pro:Cit-NLS
Plastid
Air pore
100 µm

Fig. 2

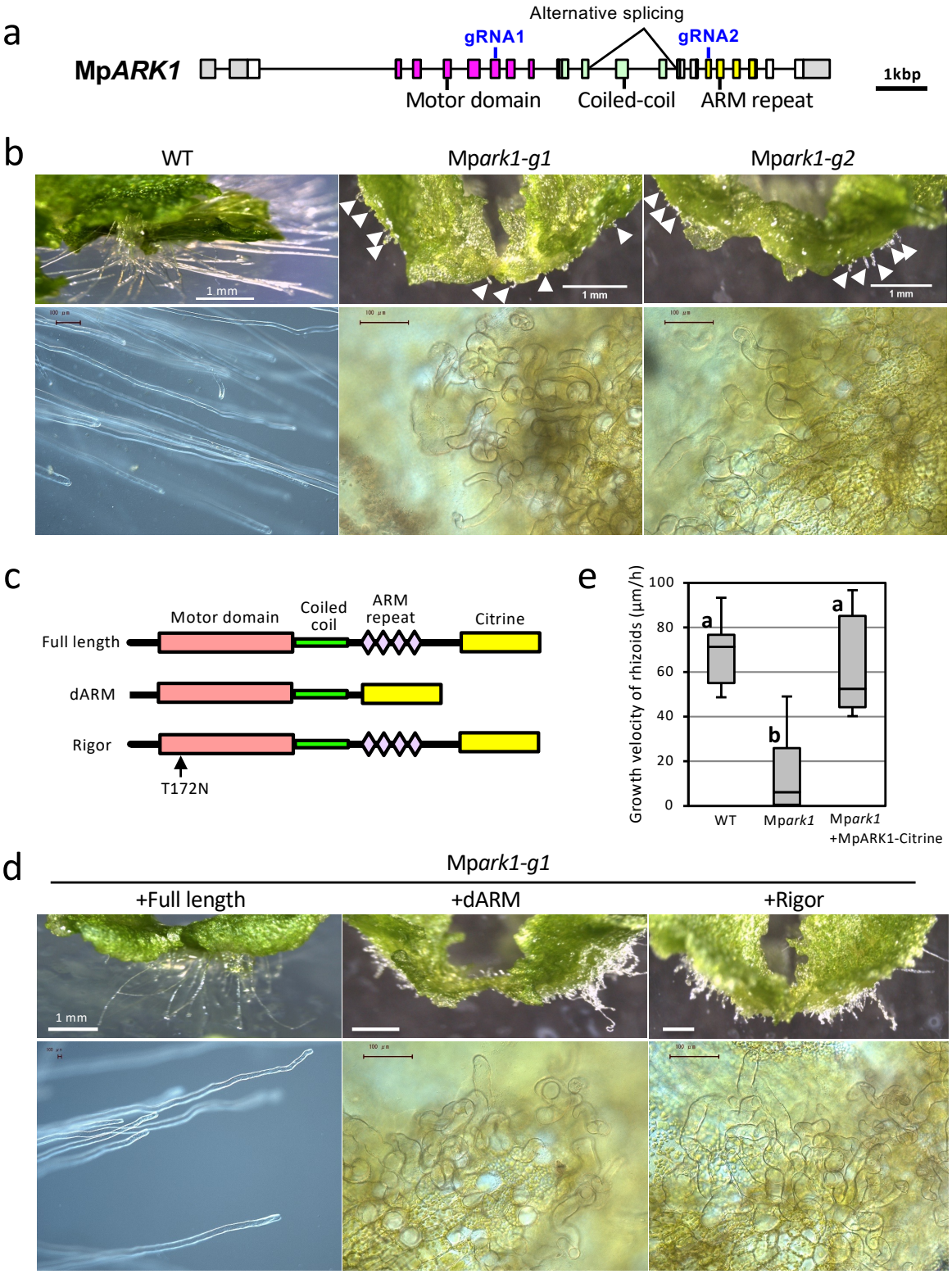
a
Alternative splicing
gRNA1
gRNA2
MpARK1
Motor domain
Coiled-coil
ARM repeat
1kbp
b
WT
Mpark1-g1
Mpark1-g2
1 mm
c
Motor domain
Coiled coil
ARM repeat
Citrine
Full length
dARM
Rigor
T172N
e
Growth velocity of rhizoids (μm/h)
100
80
60
40
20
0
a
b
a
WT
Mpark1
Mpark1 +MpARK1-Citrine
d
Mpark1-g1
+Full length
+dARM
+Rigor
1 mm

Fig. 3

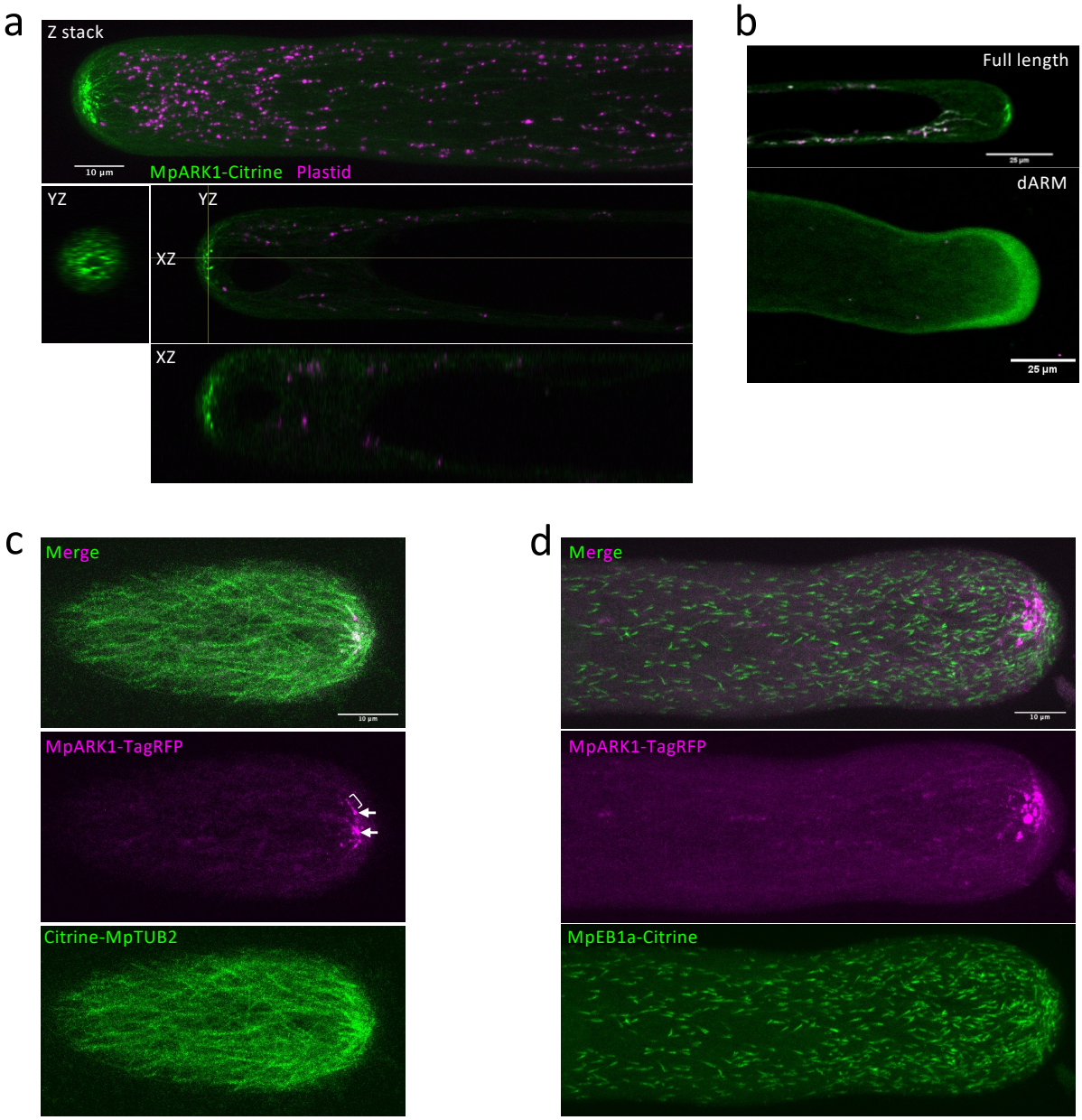
a
Z stack
10 µm
MpARK1-Citrine
Plastid
YZ
YZ
XZ
XZ
b
Full length
dARM
25 µm
c
Merge
MpARK1-TagRFP
Citrine-MpTUB2
d
Merge
MpARK1-TagRFP
MpEB1a-Citrine

Fig. 4

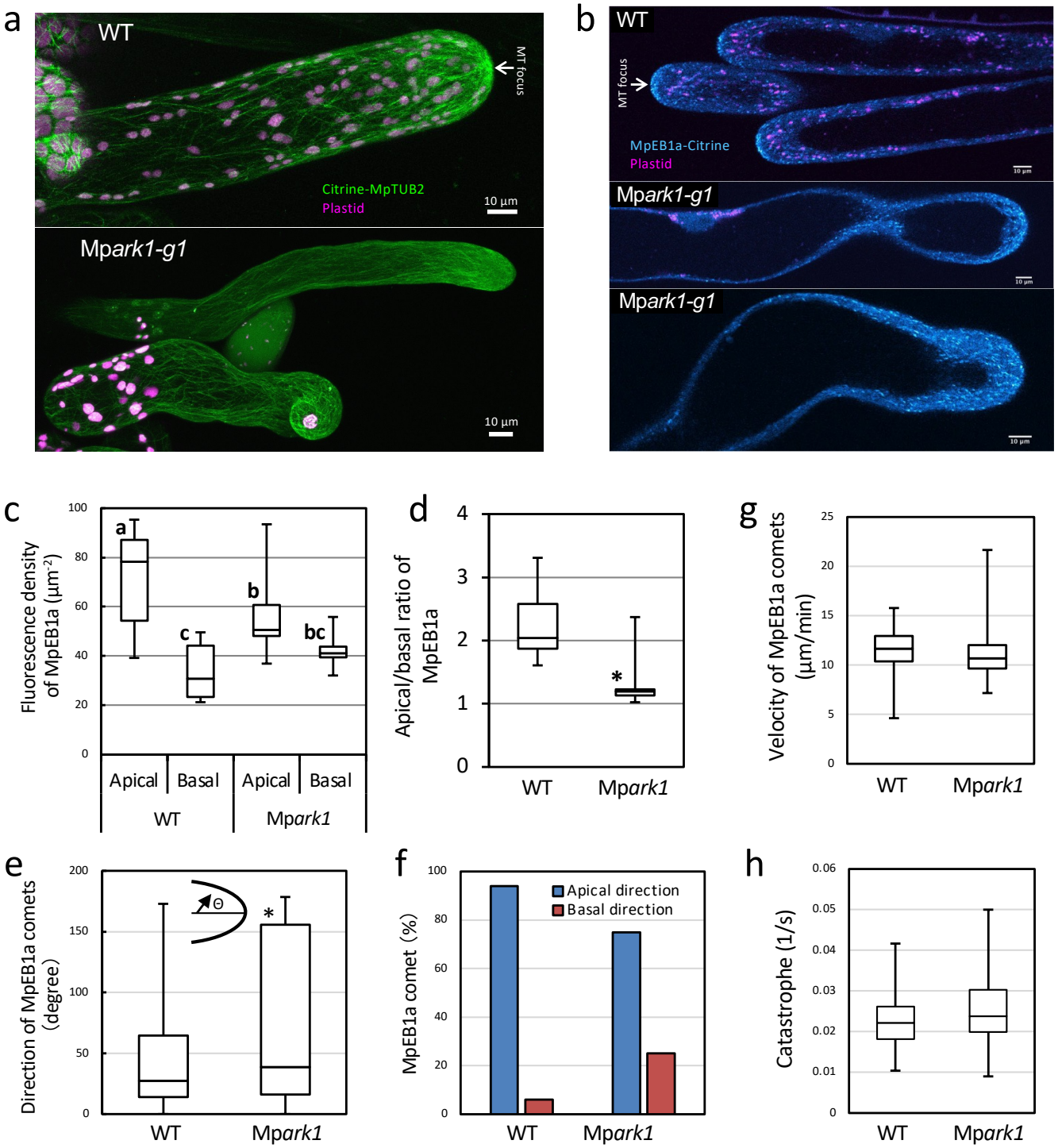
a
WT
MT focus
Citrine-MpTUB2
Plastid
10 µm
Mpark1-g1
10 µm
b
WT
MT focus
MpEB1a-Citrine
Plastid
Mpark1-g1
Mpark1-g1
c
Fluorescence density of MpEB1a (µm⁻²)
a
c
b
bc
Apical
Basal
Apical
Basal
WT
Mpark1
d
Apical/basal ratio of MpEB1a
*
WT
Mpark1
g
Velocity of MpEB1a comets (µm/min)
WT
Mpark1
e
Direction of MpEB1a comets (degree)
Θ
*
WT
Mpark1
f
MpEB1a comet (%)
Apical direction
Basal direction
WT
Mpark1
h
Catastrophe (1/s)
WT
Mpark1

Fig. 5

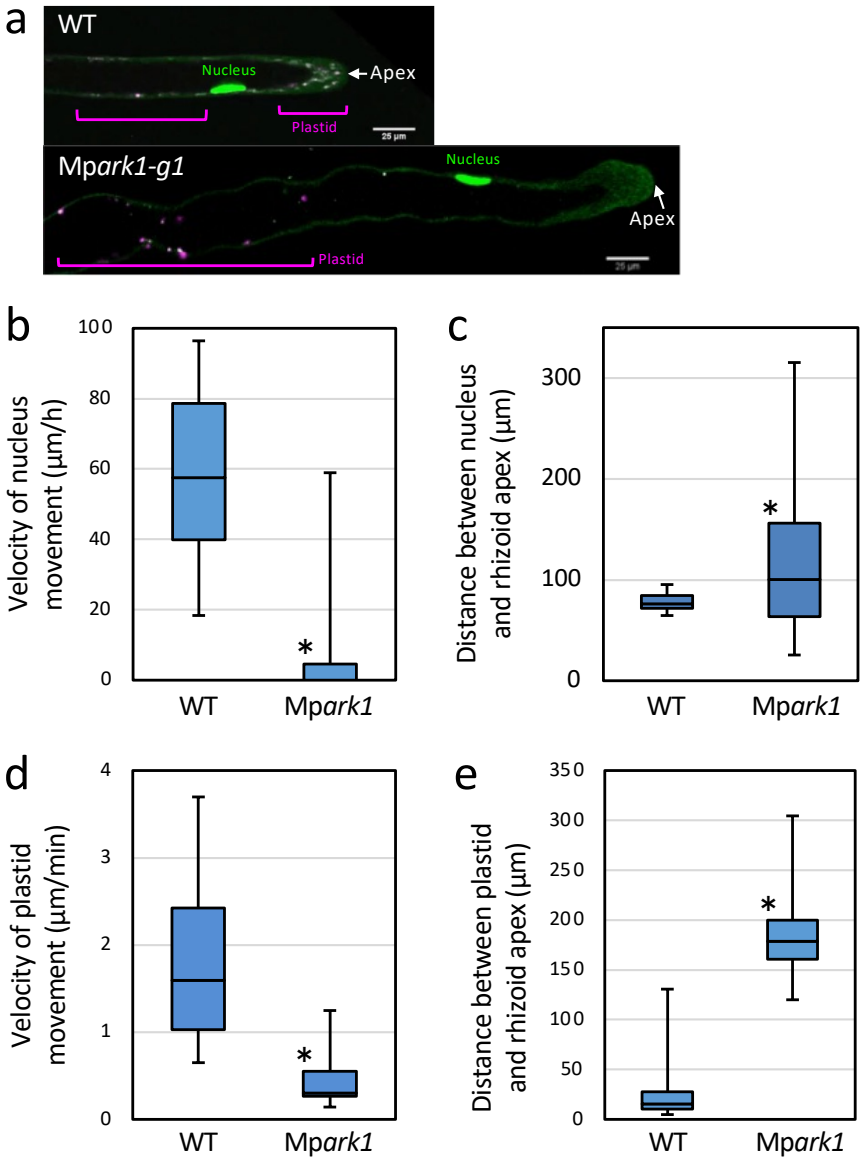
a
WT
Nucleus
Apex
Plastid
Mpark1-g1
Nucleus
Apex
Plastid
b
Velocity of nucleus movement (µm/h)
100
80
60
40
20
0
*
WT
Mpark1
c
Distance between nucleus and rhizoid apex (µm)
300
200
100
0
*
WT
Mpark1
d
Velocity of plastid movement (µm/min)
4
3
2
1
0
*
WT
Mpark1
e
Distance between plastid and rhizoid apex (µm)
350
300
250
200
150
100
50
0
*
WT
Mpark1

Fig. 6

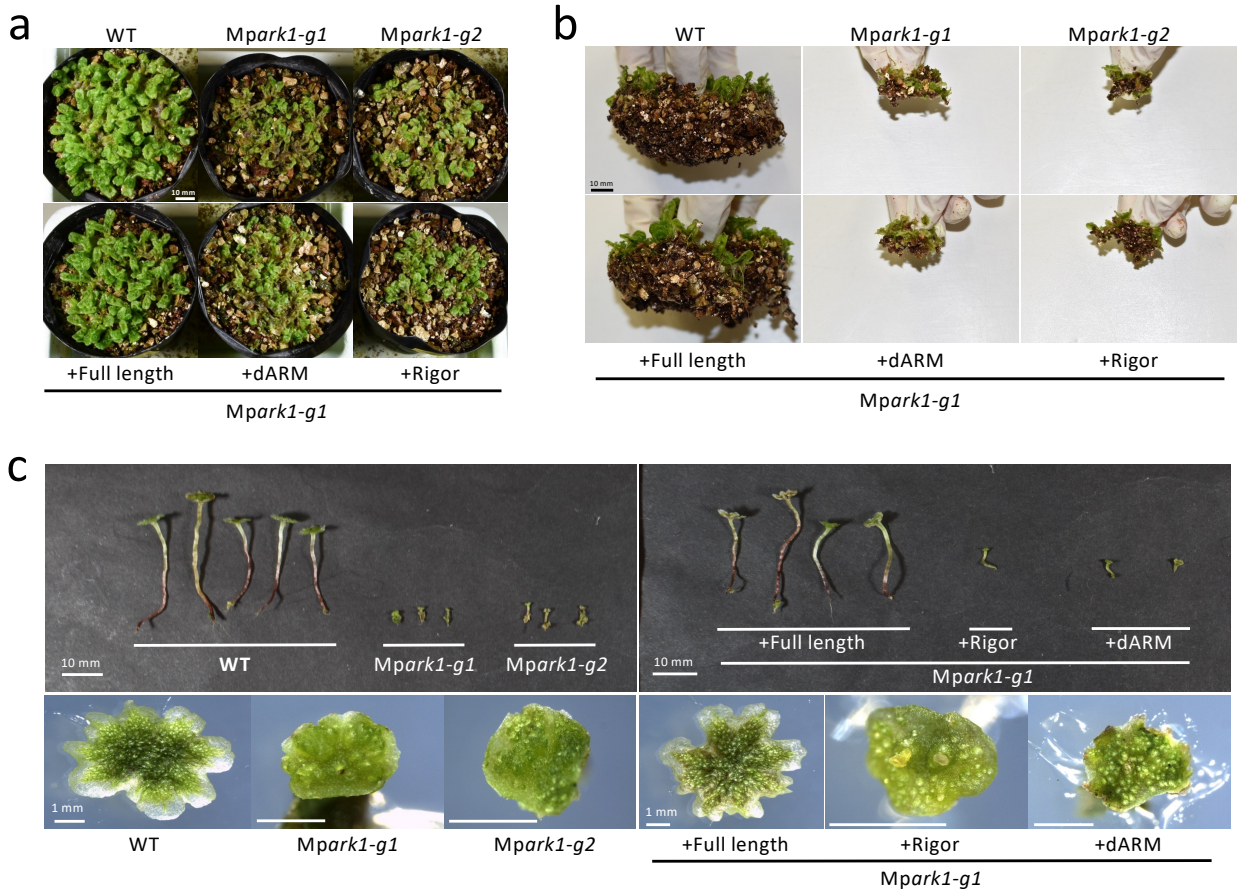
a
WT
Mpark1-g1
Mpark1-g2
10 mm
+Full length
+dARM
+Rigor
Mpark1-g1
b
WT
Mpark1-g1
Mpark1-g2
10 mm
+Full length
+dARM
+Rigor
Mpark1-g1
c
10 mm
WT
Mpark1-g1
Mpark1-g2
10 mm
+Full length
+Rigor
+dARM
Mpark1-g1
1 mm
WT
Mpark1-g1
Mpark1-g2
1 mm
+Full length
+Rigor
+dARM
Mpark1-g1

Fig. S1

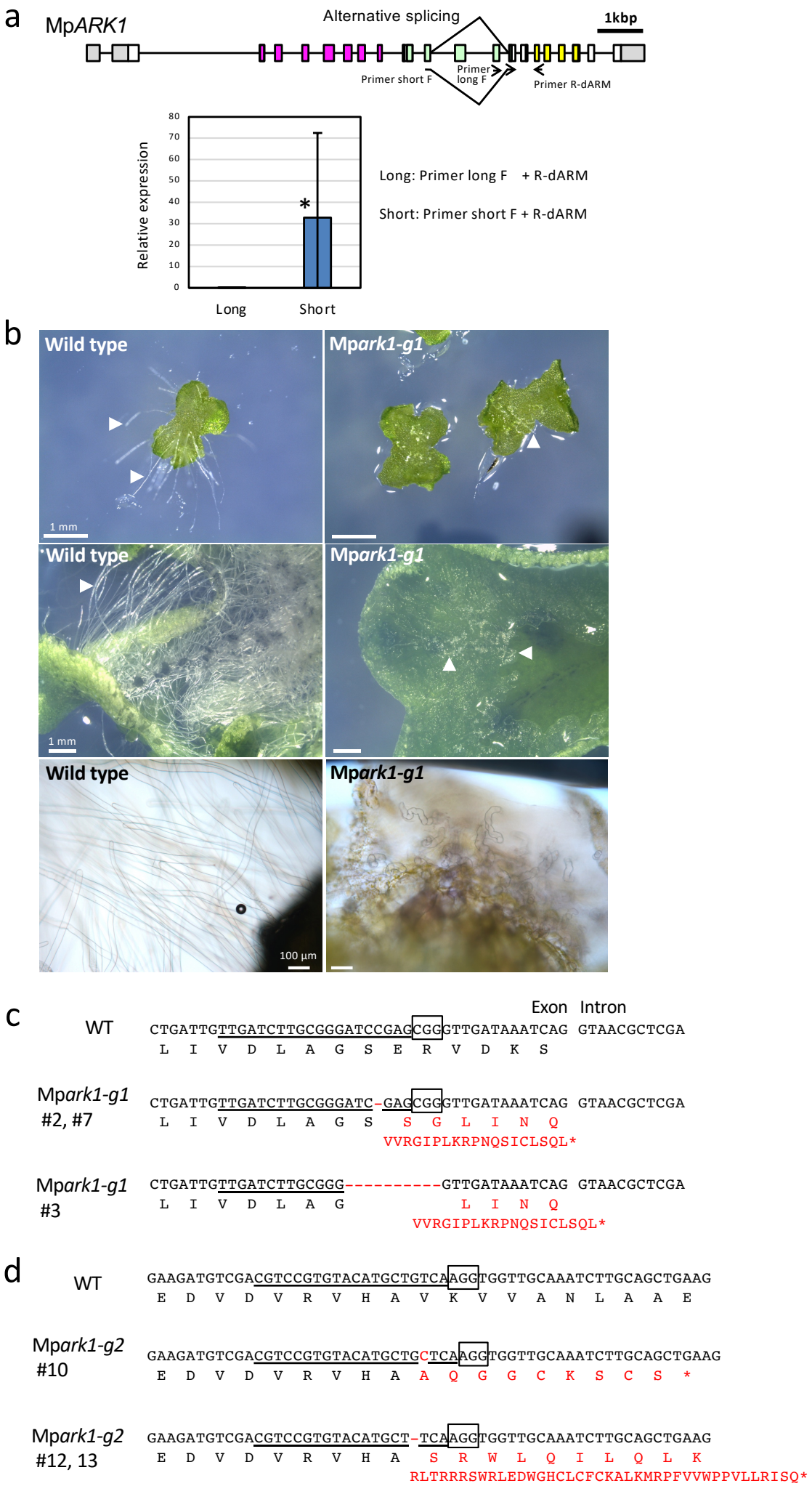

a
MpARK1
Alternative splicing
1kbp
Primer short F
Primer long F
Primer R-dARM
Relative expression
80
70
60
50
40
30
20
10
0
*
Long
Short
Long: Primer long F + R-dARM
Short: Primer short F + R-dARM
b
Wild type
Mpark1-g1
1 mm
Wild type
Mpark1-g1
1 mm
Wild type
Mpark1-g1
100 µm
c
Exon Intron
WT
CTGATTGTTGATCTTGCGGGATCCGAGCGGGTTGATAAATCAG GTAACGCTCGA
L I V D L A G S E R V D K S
Mpark1-g1
#2, #7
CTGATTGTTGATCTTGCGGGATC-GAGCGGGTTGATAAATCAG GTAACGCTCGA
L I V D L A G S S G L I N Q
VVRGIPLKRPNQSICLSQL*
Mpark1-g1
#3
CTGATTGTTGATCTTGCGGG----------GTTGATAAATCAG GTAACGCTCGA
L I V D L A G L I N Q
VVRGIPLKRPNQSICLSQL*
d
WT
GAAGATGTCGACGTCCGTGTACATGCTGTCAAGGTGGTTGCAAATCTTGCAGCTGAAG
E D V D V R V H A V K V V A N L A A E
Mpark1-g2
#10
GAAGATGTCGACGTCCGTGTACATGCTGCTCAAGGTGGTTGCAAATCTTGCAGCTGAAG
E D V D V R V H A A Q G G C K S C S *
Mpark1-g2
#12, 13
GAAGATGTCGACGTCCGTGTACATGCT-TCAAGGTGGTTGCAAATCTTGCAGCTGAAG
E D V D V R V H A S R W L Q I L Q L K
RLTRRRSWRLEDWGHCLCFCKALKMRPFVVWPPVLLRISQ*

Fig. S2

a

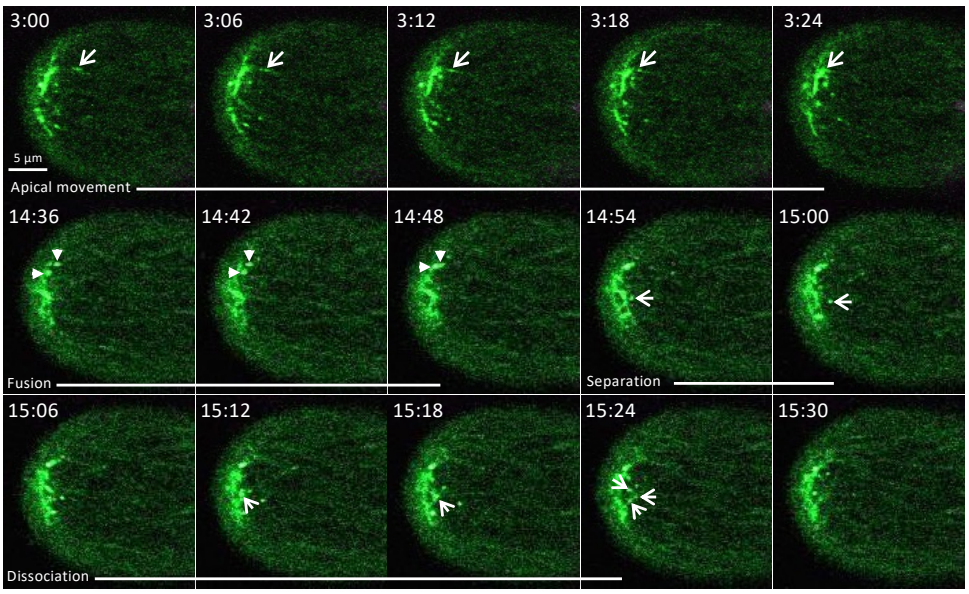
3:00
3:06
3:12
3:18
3:24
5 µm
Apical movement
14:36
14:42
14:48
14:54
15:00
Fusion
Separation
15:06
15:12
15:18
15:24
15:30
Dissociation

b

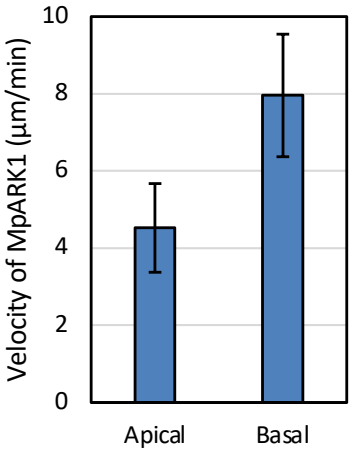
Velocity of MpARK1 (µm/min)
10
8
6
4
2
0
Apical
Basal

c

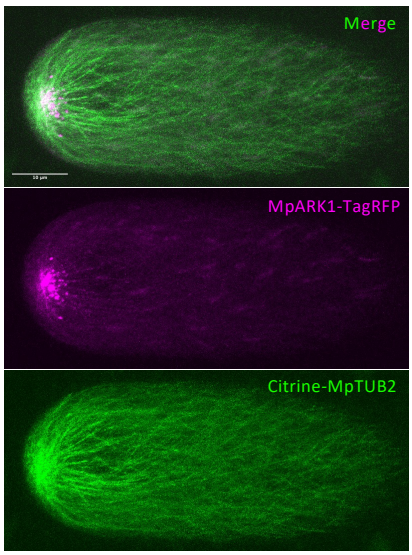
Merge
MpARK1-TagRFP
Citrine-MpTUB2

d

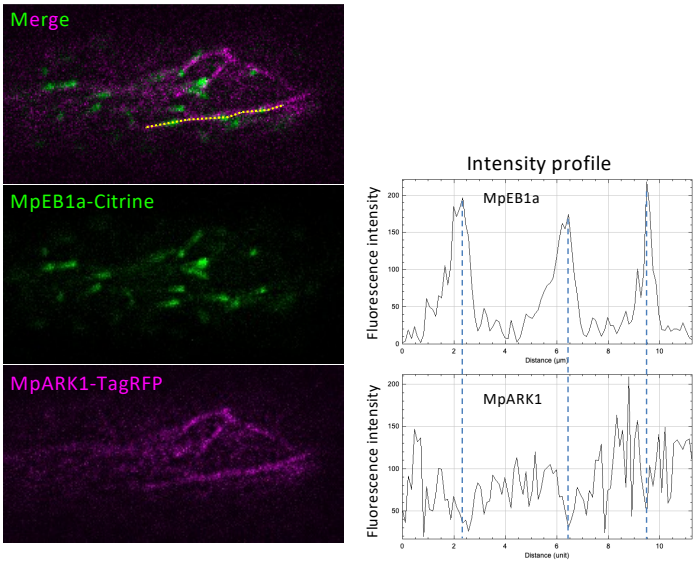
Merge
MpEB1a-Citrine
MpARK1-TagRFP
Intensity profile
MpEB1a
MpARK1
Fluorescence intensity
Distance (µm)
Distance (unit)

e

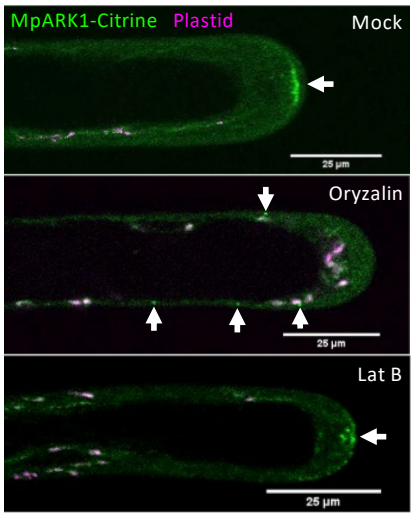
MpARK1-Citrine
Plastid
Mock
Oryzalin
Lat B
25 µm

Fig. S3

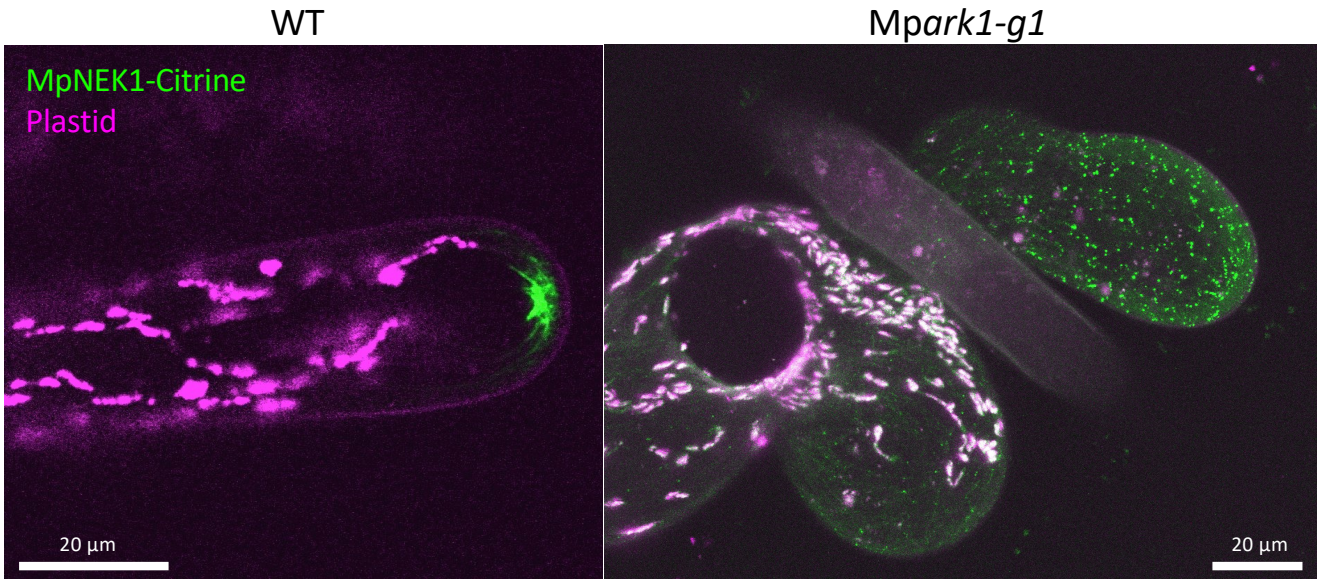

Fig. S4

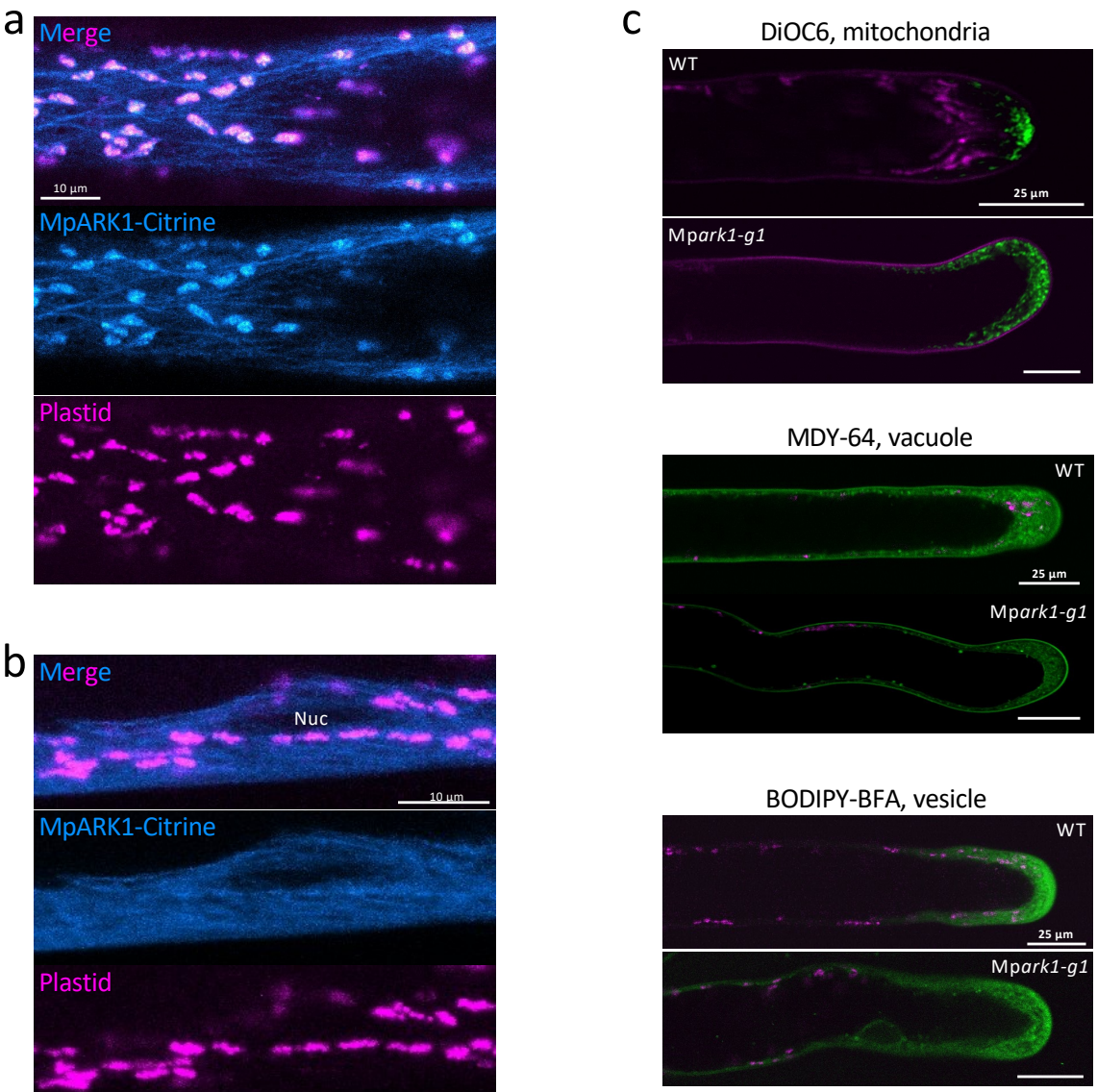
a
Merge
10 µm
MpARK1-Citrine
Plastid
b
Merge
Nuc
10 µm
MpARK1-Citrine
Plastid
c
DiOC6, mitochondria
WT
25 µm
Mpark1-g1
MDY-64, vacuole
WT
25 µm
Mpark1-g1
BODIPY-BFA, vesicle
WT
25 µm
Mpark1-g1
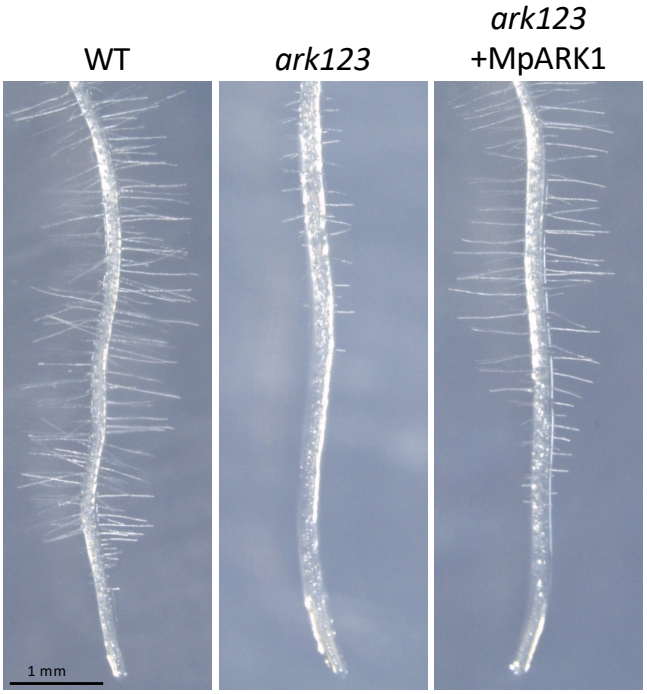
Fig. S5